JOURNAL OF GEOPHYSICAL RESEARCH, VOL. 101, NO. D22, PAGES 29,229–29,238, DECEMBER 20, 1996

Fast response resonance fluorescence CO measurements aboard the C-130: Instrument characterization and measurements made during North Atlantic Regional Experiment 1993

Christoph Gerbig, Dieter Kley, and Andreas Volz-Thomas
Institut für Chemie und Dynamik der Geosphare, Forschungszentrum Jülich, Jülich, Germany

Joss Kent, Ken Dewey, and Danny S. McKenna
Atmospheric Chemistry Group, Meteorological Research Flight, United Kingdom Meteorological Office
Farnborough, Hampshire, England

Abstract. The resonance fluorescence instrument for the measurement of atmospheric CO described by *Volz and Kley* [1985] was characterized in the laboratory and adapted for use on aircraft. A major finding was that the background signal is largely due to continuum resonance Raman scattering by molecular oxygen and thus cannot be reduced by better design. The instrument was deployed on the United Kingdom Meteorological Office (UKMO) C-130 Hercules during August 1993 and in subsequent missions. The instrument achieved a detection limit (3σ) of 5 ppb at a time resolution of 30 s. For a typical CO concentration of 100 ppb, the signal-to-noise ratio (1σ) was 15 for an integration time of 2 s, which was the minimum time resolution that could be obtained during the flights because of limited pump capacity. Data collected over the North Atlantic show distinct layers of CO above the atmospheric boundary layer (ABL) that are well correlated with enhanced NO_y mixing ratios and indicate transport of pollution from the American continent. Such layers, albeit much less pronounced, were encountered in westerly flow in the midtroposphere west of the coast of Portugal. Fairly high mixing ratios were observed in the lower troposphere associated with transport from southern Europe.

Introduction

Carbon monoxide is involved in the photochemical cycles that control the concentrations of ozone and hydroxyl radicals (OH) in the troposphere. The hydroxyl radical is responsible for the oxidative removal of CO and many other trace gases in the atmosphere. Anthropogenic emissions, in particular automobile exhaust, constitute a major source of CO in the troposphere [*Seiler*, 1974; *Logan et al.*, 1981]. Because of its photochemical lifetime of about 1 month in summer [*Volz et al.*, 1981] and because it is not removed by rainout or washout, CO is a suitable tracer to investigate the transport of polluted air masses into cleaner regions [*Fishman and Seiler*, 1983]. Because of the coemission of CO and other precursors of photochemical O_3 production, in particular NO_x, the amount of ozone that is transported from polluted areas to remote regions can be estimated from observed correlations between O_3 and CO concentrations [*Parrish et al.*, 1993]. Since a large fraction of the transport may occur above the planetary boundary layer [*Pickering et al.*, 1992], aircraft measurements are needed in order to obtain a better experimental database for estimation of the total amount of ozone and precursors that is transported to the North Atlantic region from North American sources. CO can also serve to identify air masses of stratospheric origin, in addition to measurements of H_2O [*Hipskind et al.*, 1987].

Airborne CO measurements are often made off-line, that is, in whole air samples that are collected during the flights. The most common technique is gas chromatography [cf. *Heidt*, 1978], which was also applied for in situ measurements [*Marenco et al.*, 1989]. Continuous monitoring techniques that have been used for in situ measurements of CO aboard aircrafts are the HgO method [*Seiler et al.*, 1980] with a time resolution of about 30 s, infrared absorption by gas filter correlation (GFC) [*Dickerson and Delany*, 1987] with a response time of 30 s, and tunable diode laser absorption spectroscopy (TDLAS) with a response time of 1 s [*Sachse et al.*, 1987]. The latter is the only technique used so far that combines high precision and a good time resolution.

Another promising technique for fast and sensitive CO measurements is resonance fluorescence (RF) in the fourth positive band of CO. Such an instrument was described by *Volz and Kley* [1985]. It was designed for balloon borne measurements in the stratosphere, but actually was never used for atmospheric measurements, although the instrument achieved much better sensitivity and time resolution than the GFC and has less logistic demands than TDLAS.

We have adopted the balloon instrument described by A. Volz and D. Kley and have made adjustments to use the instrument aboard the research aircraft C-130 Hercules of the Meteorological Research Flight (MRF) of the United Kingdom Meteorological Office (UKMO). Several improvements

Paper number 95JD03272.
0148-0227/96/95JD-03272$09.00

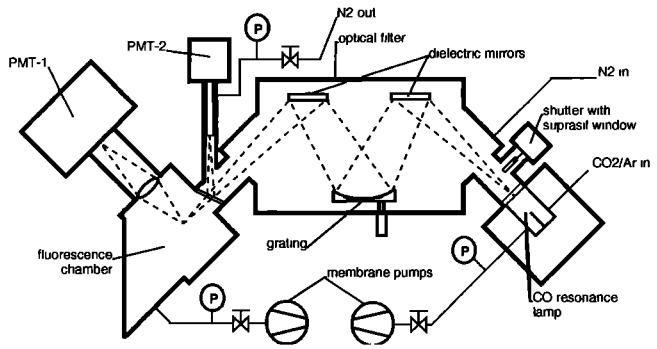

Figure 1. Schematics of the laboratory setup.

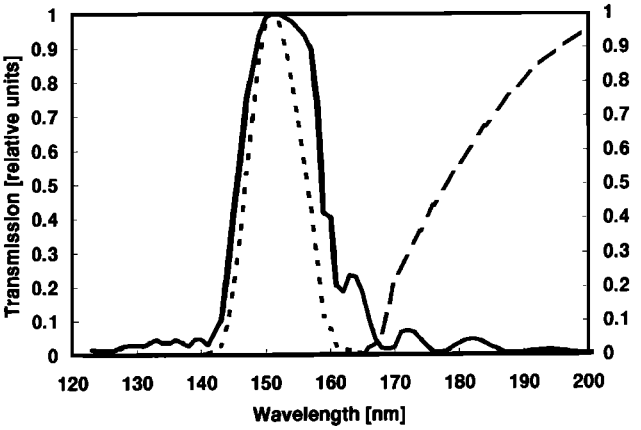

Figure 2. Spectral transmission of the optical filter with the grating (solid line) in zeroth order and (dotted line) first order. Also shown is (dashed line) the spectral transmission of the fluorescence detection.

were made to the original instrument in order to reduce the weight and to achieve a better detection limit. The instrument was characterized in the laboratory and was flown for the first time aboard the C-130 during the North Atlantic Regional Experiment (NARE) summer campaign in 1993.

Laboratory Tests and Assessment of Performance

The basic mechanism of the CO measurement by RF is given by reactions (R1) to (R3). Excitation of atmospheric CO occurs in (R1) by radiation from a CO resonance lamp after having selected the appropriate wavelength interval by means of an optical filter. Besides the fluorescence (R2), the excited CO molecule is also deactivated by collisions with other molecules; for example, N_2 and O_2 (R3).

$$CO\left(X^1\sum, v''=0\right) + h\nu \mapsto CO\left(A^1\prod, v'\right) \quad \text{(R1)}$$

$$CO\left(A^1\prod, v'\right) \mapsto CO\left(X^1\sum, v''\right) + h\nu \quad \text{(R2)}$$

$$CO(A^1\prod, v') + M \mapsto CO(X^1\sum, v'') + M \quad \text{(R3)}$$

The schematics of the RF instrument described by *Volz and Kley* [1985] are given in Figure 1. Briefly, it consists of a resonance lamp, a fluorescence chamber, and an optical filter, that is, a folded Seya Namioka monochromator with a holographic grating ($f/4.5$, 1200 lines mm^{-1}) and two dielectric mirrors that serve to further reduce the bandwidth of the filter. The spectral transmission of the optical filter is given in Figure 2 for two different configurations, grating in first order and grating in zeroth order. It is centered at the strongest emission band of the CO lamp (1–0, λ = 151 nm) and has a bandwidth of 9 nm (full width at half maximum (FWHM)) with the grating in first order and a bandwidth of 12 nm (FWHM) without the grating. Because of the strong absorption that O_2 has in the spectral region of 150 nm, the optical filter is continuously flushed with a small flow of N_2 (50 mL/min STP, purity 99.999%), which is purified from traces of CO, CO_2, and H_2O by passing it over a bed of hopcalite and molecular sieve. The fluorescence is most intense in the wavelength range from 170 to 200 nm; see *Volz and Kley* [1985]. It is detected with a photomultiplier tube (PMT) (Hamamatsu R759, CsTe cathode) through a $f/1$ suprasil lens. The spectral response of the detection system is also shown in Figure 2. A second PMT (Hamamatsu R1081, CsI cathode) is used to monitor the intensity of the exciting radiation at the exit window of the optical filter.

Optimization of the Resonance Lamp

The microwave discharge lamp of the original instrument was replaced by a radio frequency discharge lamp (Quantatec) in order to save weight, space, and energy. The lampbody was modified to allow flow-through operation. The resonance lamp is operated with a mixture of CO_2 in Ar at a pressure of 5–10 mbar [*Fink*, 1976]. Optimization of the lamp parameters (flow, pressure, CO_2 mixing ratio) was achieved by monitoring of the fluorescence of 5 ppm CO in air and CO-free air, respectively, while the different parameters were varied. The best sensitivity was obtained with a mixture of 0.25% CO_2 in Ar. The pressure dependence of the sensitivity for CO, the background signal, expressed in CO equivalents, and the reference signal (PMT 2) is shown in Figure 3. For these experiments, the mass flow was maintained at 40 mL/min STP. It is seen, that the background increases steadily with pressure, whereas the sensitivity decreases at higher pressures. The largest signal-to-noise ratio is obtained at a lamp pressure of 8 mbar. The optimum pressure depends on flow rate and, hence, on the capacity of the pump. Without limited pump efficiency, the intensity of the lamp increases with increasing flow rate. The reason is that the CO emission is partially absorbed in the lamp itself by ground state

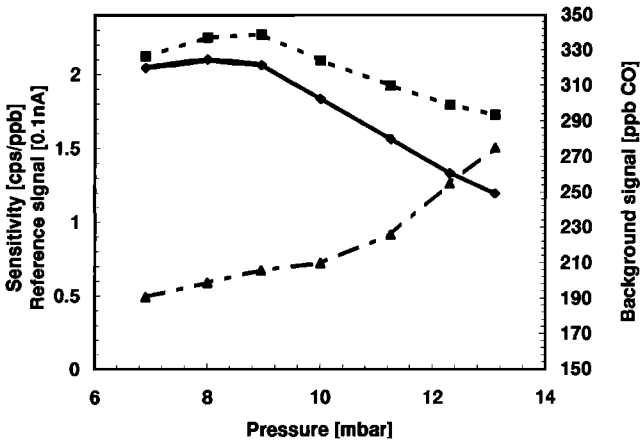

Figure 3. (diamonds) Sensitivity, (squares) reference signal, and (triangles) background signal as function of the pressure in the discharge lamp.

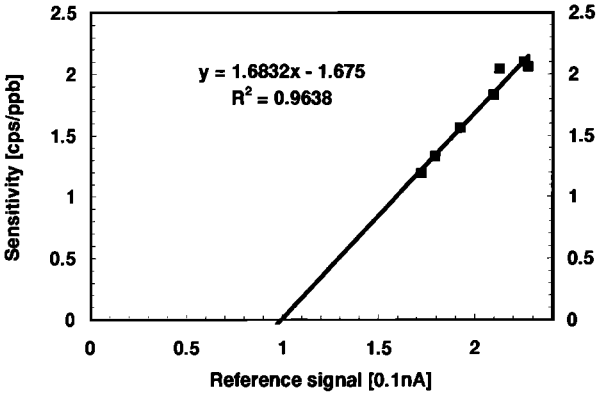

Figure 4. Relation between sensitivity and reference signal for changes in lamp pressure.

CO molecules that arise from the decomposition of the CO_2. The concentration of CO in the lamp depends at first approximation inversely upon flow rate. The flow rate of 40 mL/min STP was chosen to match the capacity of the pump used during the airborne measurements (see below).

Figure 3 also shows the dependence of the reference signal (PMT 2) on pressure. It exhibits a similar, albeit much weaker, pressure dependence. This is more clearly seen in Figure 4, which shows a scatter diagram of the instrument's sensitivity as function of the reference signal for pressure changes in the lamp. The two variables are not directly proportional, with the reference signal decreasing more slowly than the sensitivity. Reasons for this behavior are that the quantum yield of PMT 2 is almost constant over the range of the fourth positive band of CO, whereas the CO absorption spectrum consists of narrow rotational lines. While the reference signal is a measure of the integral intensity of the CO lamp at the entrance to the fluorescence chamber, the fluorescence intensity of CO depends strongly on line width and rotational distribution of the lamp's emission spectrum. For example, pressure broadening in the lamp causes a decrease in sensitivity, but leaves the total emission intensity almost unchanged. Likewise, self absorption, that is, by CO molecules in the discharge, reduces mainly the emission lines with $v'' = 0$, which are responsible for excitation of the atmospheric CO (higher vibrational states are not occupied at room temperature), and affects the total output of the lamp to a lesser extent.

A similar behavior was found for changes in lamp temperature. The resonance fluorescence signal decreased at a rate of $-1.2\%/°C$ with increasing temperature, while the reference signal decreased only at $-0.5\%/°C$. The decrease in lamp intensity is mainly due to a decreasing radio frequency output of the transmitter with increasing temperature. Another reason, although of lesser importance, is Doppler broadening of the rotational lines and changes in the population of the rotational levels with changing lamp temperature. The only parameter that produced proportional changes in sensitivity and reference signal is the supply voltage for the radio frequency circuit, a parameter, which is easy to control. Since under normal operating conditions, all parameters may vary simultaneously, a correction of the resonance fluorescence signal with the help of PMT 2, as suggested by A. Volz and D. Kley, is not possible. In order to maintain a stable sensitivity, it is necessary to control the relevant lamp parameters, that is, pressure, flow rate, temperature, and the supply voltage.

Influence of Oxygen

The signal measured by PMT 1 consists not only of the resonance fluorescence from CO (R2), but also of a so-called background signal, which is determined when CO-free air is sampled. The achievable signal-to-noise ratio (S/N, equation (1)) depends on two quantities: the sensitivity, S_{CO} (i.e., the count rate per ppb CO) and magnitude of the background signal B in c/s. (B/S_{CO} is the background signal in CO equivalents, and μ_{CO} is the mixing ratio of CO). Under the assumption that the count rates follow a Poisson distribution, the signal-to-noise ratio is

$$\frac{S}{N} = \frac{S_{CO} \cdot \mu_{CO}}{\sqrt{S_{CO} \cdot \mu_{CO} + 2B}} = \sqrt{S_{CO}} \frac{\mu_{CO}}{\sqrt{\mu_{CO} + 2B/S_{CO}}} \quad (1)$$

At high CO concentrations, B/S_{CO} can be neglected against μ_{CO} and the signal-to-noise ratio depends only on the sensitivity, that is,

$$\frac{S}{N} = \sqrt{S_{CO} \cdot \mu_{CO}} \quad (2)$$

At low concentrations, however, the background signal becomes important since S/N decreases with the square root of B

$$\frac{S}{N} = \frac{S_{CO} \cdot \mu_{CO}}{\sqrt{2B}} \quad (3)$$

In addition, any drift in the background signal produces an uncertainty in the CO determination above the statistical error. For example, with a background signal of $B/S_{CO} = 1$ ppm, background fluctuations between two subsequent background determinations must be <0.1%, in order to achieve an accuracy of 1 ppb.

The background consists of the dark current of PMT 1 (10 c/s) and a contribution that arises from elastic scattering of photons on the walls of the fluorescence chamber and on gas molecules (Rayleigh scattering). The contribution from elastic scattering is minimized by proper design of the fluorescence chamber and by separation of the spectral ranges of excitation and fluorescence detection at about 160 nm (see Figure 2). Hence elastic scattering is relevant only for photons with $\lambda >$ 160 nm. However, a background signal can also be caused by photons with $\lambda <$ 160 nm due to inelastic scattering on molecules other than CO.

Volz and Kley [1985] suggested to monitor the background, in addition to the measurement of CO-free air, by moving a suprasil window into the light path of the resonance lamp. The window absorbs radiation from the lamp at wavelengths <160 nm, so that the fluorescence is reduced by more than 3 orders of magnitude, and leaves the intensity at wavelengths >160 nm nearly unchanged. (The optical thickness of the additional window (1 mm) is small compared to that provided by the suprasil lens and the PMT window (>5 mm)). The remaining signal should thus be a measurement of stray light that arises from elastic scattering. The window can be moved in and out of the light path at time intervals of <1 s without affecting the sample gas flow.

We have made several tests for investigation of the origin of the background signal. The fluorescence signal was measured in different gases, while the suprasil window was moved in and out of the light path between lamp and optical filter. A summary of the results is given in Table 1. With the suprasil

Table 1. Fluorescence Signals Obtained in Different Gases With and Without Window

Gas	Without Window	With Window
1 ppm CO in zero air	2610 ± 30 c/s	12 ± 1 c/s
Zero air	110 ± 2 c/s	12 ± 1 c/s
N_2	25 ± 1 c/s	nanometer

The dark current was subtracted from all signals.

window in the light path, the fluorescence signal obtained in a mixture of 1 ppm CO in air is exactly the same as that in zero air, which confirms that the radiation from the lamp in the region responsible for the excitation of CO is indeed fully absorbed. The signal obtained in CO-free air without the window, however, is almost 1 order of magnitude larger than that with the window in place. When the fluorescence chamber is flushed with pure N_2 instead of zero air, again a much smaller signal is observed. The higher signal in N_2 than that in air with the window can be explained by the fact that the excitation radiation is strongly absorbed by molecular oxygen in the Schumann Runge continuum ($\sigma = 1.1 \times 10^{-17}$ cm^2/mol at 150 nm; *Herzberg* [1974]).

The results in Table 1 suggest that a large fraction of the background signal must be due to inelastic scattering by oxygen molecules. A mechanism that can explain the observations is continuum resonance Raman scattering. Figure 5 shows the potentials of the relevant electronic states of O_2. When a photon is absorpted by an O_2 molecule (R4) there is a certain probability not only for dissociation (R5), but also for transition to the ground state by emission of a photon (R6).

$$O_2(X^3\Sigma_g^-) + h\nu(\lambda = 150\text{ nm}) \mapsto O_2(B^3\Sigma_u^-) \quad \text{(R4)}$$

$$O_2(B^3\Sigma_u^-) \mapsto O(^3P) + O(^1D) \quad \text{(R5)}$$

$$O_2(B^3\Sigma_u^- \mapsto O_2(X^3\Sigma_g^-) + h\nu(629 \geq \lambda \geq 150\text{ nm}) \quad \text{(R6)}$$

The ratio between the probabilities for dissociation and emission can be roughly estimated from the product of the duration of a vibration of the $B\ ^3\Sigma_u^-$ state (about 10^{-13} s) and the Einstein coefficient for (R6), which should be around 10^7 s^{-1} for an allowed transition at 150 nm. This gives a fluorescence yield of about 10^{-6}, if quenching is neglected. The emission extends to longer wavelengths, because the transition (R6) may occur into higher vibronic levels of the ground state.

Table 2. Fluorescence Signals, Detection Limit, and Signal-to-Noise Ratios Obtained With Grating in First Order and in Zeroth Order

	First Order	Zeroth Order
Signal of 1 ppm CO in air	2610 c/s	6900 c/s
Signal of CO-free air	110 c/s	900 c/s
Detection limit (1-σ)	6.2 ppb s$^{1/2}$	7.1 ppb s$^{1/2}$
S/N at 50 ppb	6.5 s$^{-1/2}$	6.5 s$^{-1/2}$
S/N at 100 ppb	11.3 s$^{-1/2}$	12.2 s$^{-1/2}$
S/N at 500 ppb	32.4 s$^{-1/2}$	43.2 s$^{-1/2}$

Since the fraction of the background that is caused by O_2 has a similar spectral distribution, it cannot be distinguished from the CO fluorescence and, hence, cannot be reduced relative to the CO signal by using a better spectral separation between excitation and detection. On the other hand, if background and CO signal vary proportionally with lamp intensity, the signal-to-noise ratio increases with the square root of the intensity. It was, therefore, investigated if the signal-to-noise ratio could be improved by operating the optical filter without the grating (i.e., using the zeroth order). The signals obtained for zero air and the CO mixture with the two different configurations are shown in Table 2, together with the signal-to-noise ratio that was calculated for different CO concentrations under the assumption that counting statistics were the only source of uncertainty.

The fluorescence signal obtained from 1 ppm CO in air is about a factor of 2.4 higher in zeroth order than in first order. This is mainly due to the low efficiency of the holographic grating in the first order. Another reason is the narrower bandwidth in the first order, which reduces the intensities of the 0–0 band at 154.4 nm and the 2–0 band at 147.8 nm. The signal measured in CO-free air increases by a factor of 8.2, between first and zeroth order. The background expressed in CO equiv-

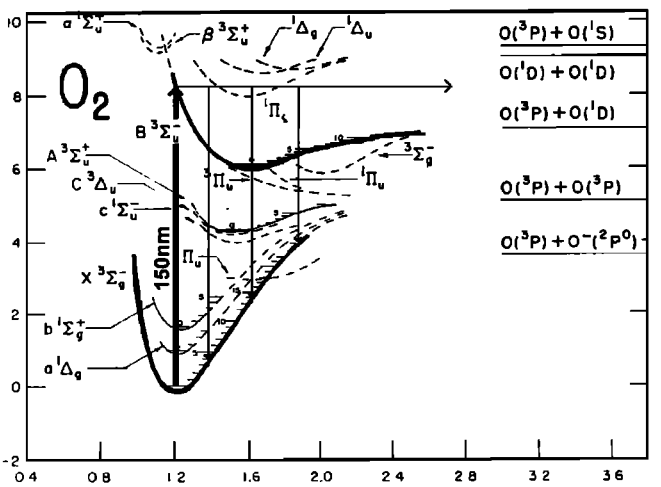

Figure 5. Potential curves of molecular oxygen (adapted from *Krupenie* [1972]). The thick arrow indicates the transition due to absorption of a photon at a wavelength around 150 nm. Possible radiative transitions to the ground state are indicated by the thin arrows.

alents, however, changes only by a factor of 3.4, that is, from 50 ppb to 150 ppb. In summary, the detection limit is somewhat better with the narrower bandwidth, but the signal-to-noise ratio above a CO mixing ratio of 50 ppb is better without the grating.

Clearly, the higher sensitivity is mainly due to the low efficiency of the holographic grating in the existing instrument. The use of a more efficiently blazed grating would increase the light intensity by about a factor of 3. It is conceivable that a sufficient signal-to-noise ratio can be obtained by using a monochromator without the dielectric mirrors.

Another possibility to simplify the optical filter is to use only the dielectric mirrors for wavelength selection (as is effectively done when using the grating in zeroth order). In fact, we have redesigned the optical filter after the flights were made. In our new design, the lamp is imaged into the fluorescence chamber by means of two $f/1.8$ CaF_2 lenses, with the two dielectric mirrors placed in the parallel part of the light beam. Because of the larger aperture and the better geometry (round apertures instead of a slit) of the imaging system, this design, in addition to being smaller, achieves a much higher sensitivity and a better signal-to-noise ratio [*Zöller*, 1995].

Influence of Water Vapor

Interferences by NO, NO_2, and CO_2 were investigated by *Volz and Kley* [1985] and found to be negligible under atmospheric conditions. We have confirmed their results for CO_2 and made additional experiments to investigate the influence of water vapor on the measurement, using both settings of the grating. In the original configuration (grating in first order), a mixing ratio of 2% H_2O causes a decrease in the fluorescence signal of 10%, as compared to dry air. H_2O has a strong absorption in the vacuum UV at $\lambda < 185$, with a broad maximum at 165 nm of about 100 cm^{-1} and a minimum at 145 nm [*Watanabe and Zelikoff*, 1953]. Therefore the interference is mainly due to absorption by H_2O of the CO fluorescence, in particular, since the distance over which the absorption occurs is about 8 cm as compared to 2 cm for the excitation radiation (see Figure 1).

When using the grating in zeroth order, the addition of 2% H_2O produces a fluorescence signal, that is equivalent to 600 ppb of CO. This positive interference is caused by photodissociation of H_2O (R7) and subsequent fluorescence of the excited OH radicals (R8) at wavelengths around 310 nm [*Terenin and Neuimin*, 1934].

$$H_2O + h\nu \mapsto OH\left(A^2 \overset{+}{\Sigma}\right) + H(^2S) \qquad (\lambda < 137 \text{ nm}) \qquad \text{(R7)}$$

$$OH\left(A^2 \overset{+}{\Sigma}\right) \mapsto OH\left(X^2 \prod\right) + h\nu \qquad \text{(R8)}$$

Energetically, excited OH molecules can be formed in the photolysis of H_2O at wavelengths below 137 nm. When using the grating in first order, the transmission of the optical filter below 137 nm is almost zero (Figure 2), in accordance with the experimental finding that a fluorescence signal from H_2O is not observed. With the grating in zeroth order, however, the transmission of the optical filter at $\lambda < 137$ nm is a few percent, which explains the observed fluorescence from H_2O. To eliminate the interference of water vapor below a CO equivalent of 1 ppb, the atmospheric water vapor must be reduced to a level below 20 ppm, which is easily achieved by passing the sample air through a cold trap or a over bed of Drierite ($CaSO_4$ with humidity indicator or Sicapent (P_2O_5 with humidity indicator). Despite the larger chances for interferences by H_2O, we have chosen to use the grating in zeroth order because of the better signal-to-noise ratio, in particular, since the water had to be removed in any case for application in the troposphere.

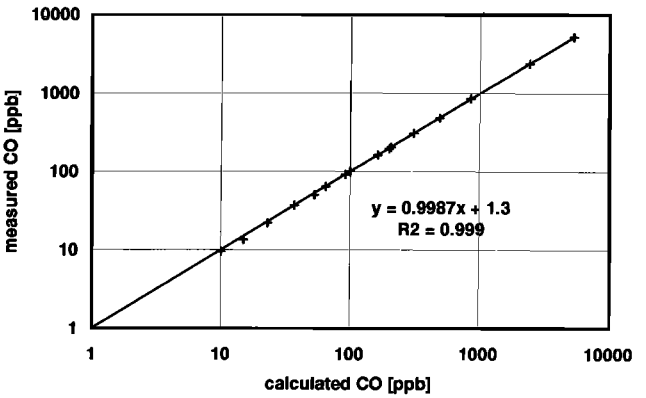

Figure 6. Linearity of the resonance fluorescence detector. The different mixing ratios were made by dynamic dilution of a standard (5.2 ppm CO in air).

The efficiency of the Sicapent trap was investigated before and during the flights by adding water vapor to standard mixtures and zero air. With the trap in place, the interference signal for a mixing ratio of 2% H_2O decreased from 600 ppb to values below 1 ppb CO equivalents. Absorption of CO by the drying agent was not observed within the experimental uncertainties (1%). Likewise, the trap did not measurably deteriorate the time resolution of the instrument, that is, the response to a step function remained below 2 s.

Dynamic Range

The linearity of the CO detector was tested by dynamic dilution of a standard mixture (5.2 ppm CO in air, AIRCO) with zero air, using mass flow controllers. The results are shown in Figure 6. Over a range of mixing ratios from 10 ppb to 5 ppm, systematic deviations from a linear response were not observed within the uncertainty of the dilution factors (2%) and the precision of the RF measurement (2 ppb or 1%, whichever is greater). In addition, the RF instrument was compared to a commercial gas filter correlation (GFC) CO monitor (TE 48 S, Thermo Instrument Systems) using CO air mixtures between 350 ppb and 12 ppm. Figure 7 shows the ratio between the mixing ratios measured by the two instruments as a function of the CO mixing ratio. Each level was sampled for 5 min to account for the slower response of the commercial instrument (30 s). The error bars include the stated nonlinearity of the GFC monitor (1% of full scale) and the statistical noise of both instruments (0.2–2%).

Measurements Made During NARE 1993

The RF instrument was installed aboard the C-130 Hercules of UKMO in August, 1993 for the summer campaign of the European research project Oxidizing Capacity of Tropospheric Atmosphere (OCTA). Figure 8 shows the plumbing of the instrument. The sample air was taken from the pressure-regulated inlet manifold of the NO_y instrument [*Lerner et al.*, 1994], which was flown simultaneously. In this manifold, a

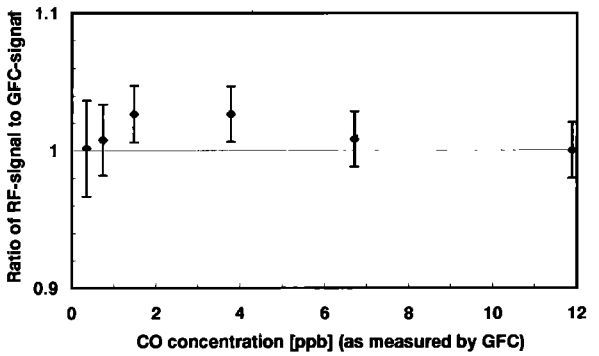

Figure 7. Comparison between the resonance fluorescence detector and a commercial gas filter correlation CO analyzer at different CO mixing ratios. Plotted are the ratios between CO measured by resonance fluorescence and CO measured by gas filter correlation. The data are averages over 4 min. Both instruments were calibrated at 0 and 12 ppm before the test.

constant pressure of 200 ± 1 mbar is maintained throughout all flight conditions. The RF instrument was connected to the inlet via a 15-m-long PFA tube of 1.6 mm inner diameter. The pressure in the fluorescence chamber was adjusted with a needle valve. A glass tube (empty volume, 6 mL) filled with Sicapent was installed in the sample line to remove water vapor. The delay time provided by the sampling line and the water trap was 9 s. It was routinely measured during calibrations and agreed well with the time lag derived from the cross correlation between CO and other trace constituents; for example, NO_y. The residence time in the inlet upstream of the manifold (1-m PFA tube of 4 mm inner diameter) is less than 0.1 s, because of the high sampling flow of the NO and NO_y instruments and the bypass pump.

Needed gases (N_2 and Ar/CO_2) were stored in 0.3 l cylinders, which were refilled before each flight. The flow rates of the gases were maintained by pressure regulators and thermostated capillaries. A membrane pump (MZ4, Vacubrand, all heads in series) was used to maintain the flow through the discharge lamp and the fluorescence chamber.

In-flight calibrations were made with a secondary standard (165 ppb CO in air). The calibration gas was injected into the sampling line, immediately behind the pressure regulated inlet, at a flow rate that was slightly higher than the sample flow rate. This procedure ensured a constant flow rate in the sampling line. The small excess flow of 10 mL/min was vented into the constant pressure manifold. Before each flight, the secondary standard was compared with a primary standard (1 ppm of CO; National Institute of Standards and Technology (NIST)). This primary standard was compared with the standard used by IFU in the EUROTRAC subproject Tropospheric Ozone Research (TOR) and with the standard used by National Center for Atmospheric Research (NCAR). The disagreement of the standards was less than 2 and 0.5%, respectively. A hopcalite scrubber was used to remove the CO from the standard for determination of the background signal. The possible error in the background measurement due to a slightly different oxygen content in the standard compared to the atmosphere was determined to be below 1 ppb CO equivalents.

The signals obtained during calibration, that is, for zero air and for a calibration gas containing 165 ppb CO, are plotted in Figure 9 for the flights A271, A272, and A273. The increase in the background signal at the beginning of flights A271 and A273 is due to contamination of the instrument with atmospheric water vapor through the exhaust pipe because of pump problems during take off. The calibration signal had the same variation superimposed. The overall variance in sensitivity was ±5% during these periods. Since the changes occur slowly, the deviation of the sensitivity from its interpolated value between calibration cycles is estimated to be less than ±2%. The background was predictable within ±2 ppb between consecutive

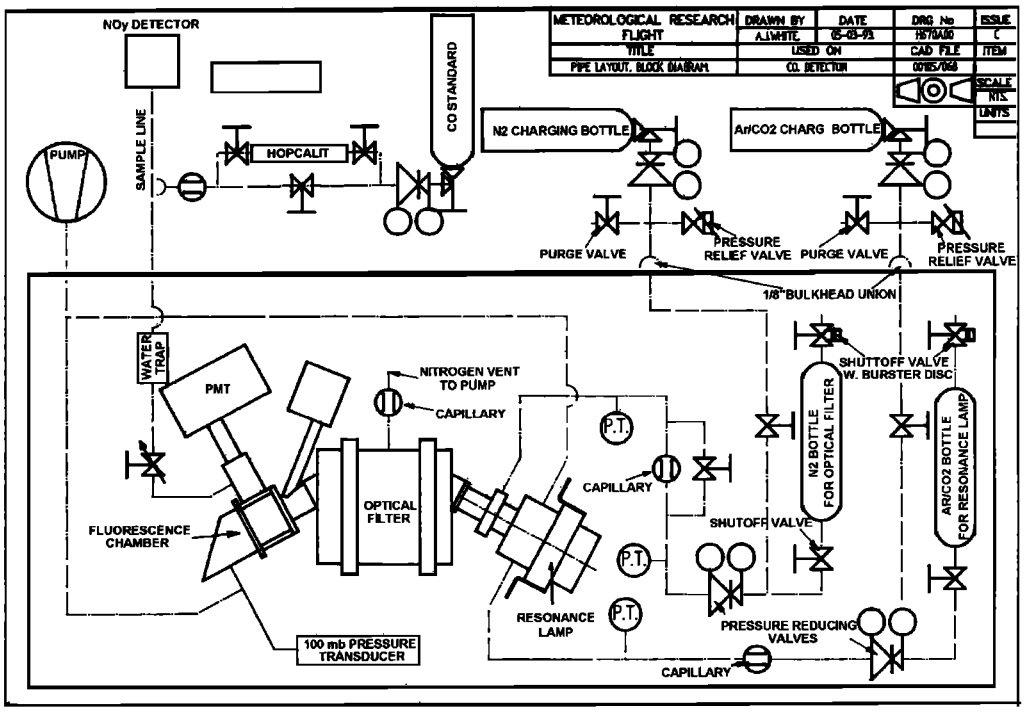

Figure 8. Block diagram of the pipe layout used for the CO detector aboard the C-130 Hercules.

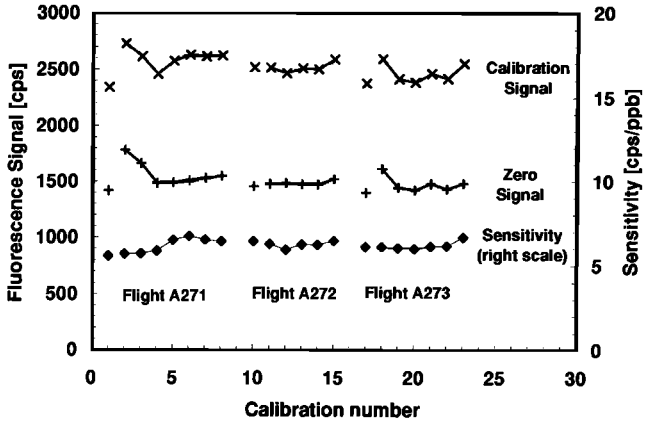

Figure 9. (crosses) Typical fluorescence signals obtained during in-flight calibrations with a secondary standard of 165 ppb CO in air and (plus sign) background signals obtained by removing the CO with a hopcalite trap. The data are averages over the calibration periods (typical duration: 1 min for calibration and zero). The time between consecutive calibration cycles is about 1 hour. The resulting sensitivity of the (diamond) instrument is plotted on the right-hand ordinate.

determinations. In flight A272, the instrument was flushed with synthetic air during take off, which prevented the initial contamination.

During the flights, the sensitivity of the instrument was 6 ± 0.3 c/s ppb and the background was about 1500 ± 90 c/s, which corresponds to 250 ppb CO. For an integration time of 1 s, a signal-to-noise ratio of 10 was obtained for an atmospheric CO mixing ratio of 100 ppb and the 3σ detection limit was about 5 ppb for an integration time of 30 s. The response time was 2 s and the delay time, because of the long sampling tube and the water trap, was 9 s. The lower sensitivity was likely due to degradation of the lamp's window within about 3 months of extensive laboratory tests.

Intercomparison With CO Measurements From Grab Samples

Carbon monoxide was measured by the Atmospheric Chemistry Group (ACG) of the UKMO by gas chromatography (Trace Analytical, model RGA 3) in whole air samples that are collected during flight. Comparison of the two measurements provides insight in the quality of the CO data, and allows identification of possible contamination in the samples, which were also used for analysis of volatile organic compounds (VOC) and organic nitrates. The CO mixture used to calibrate the RGA 3 was calibrated against our NIST standard. Because of the nonlinear response of the RGA 3, multipoint calibrations between 50 and 600 ppb were routinely made by dynamic dilution.

Figure 10a shows a scatter diagram of the CO mixing ratios measured in the bottles versus those obtained from the in situ measurement. The latter data were averaged over the time intervals in which the bottles had been filled. The error bars given for the data from the RF instrument include the precision of an individual measurement (about 1.5 ppb) and possible systematic errors from background determination (3.3 ppb) and calibration (1.5%). The uncertainty in the CO measurement from the bottles was estimated by ACG from the precision of the gas chromatography analysis to be 1 to 4%. A reduced major axis fit yields the following relation:

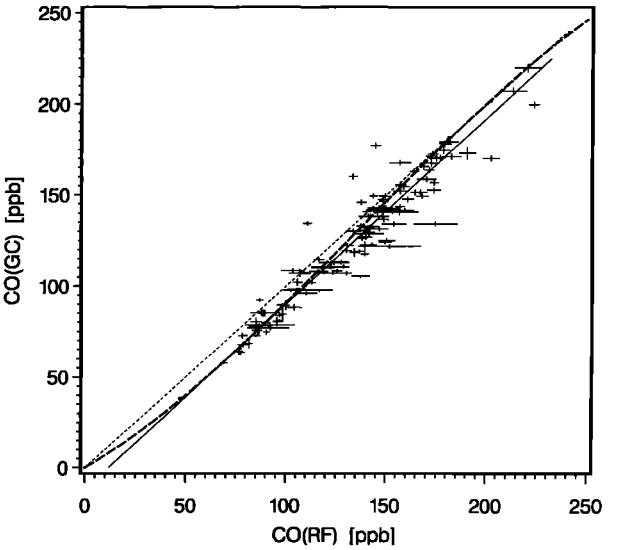

Figure 10a. Scatterplot of the CO mixing ratios obtained from gas chromatographic (GC) measurements on the whole air samples and the continuous measurements by resonance fluorescence (RF). The RF data were averaged over the sampling intervals during which the bottles were filled: solid line, linear fit; dotted line, 1:1 correlation; dashed line, polynomial fit for the nonlinear response of the RGA 3 [after *Novelli et al.*, 1994].

$$CO_{gc} = (1.022 \pm 0.027) \cdot CO_{rf} - (12.1 \pm 3.7)\ \text{ppb}$$

$$r^2 = 0.91$$

Although there is, in general, good agreement between the two measurements, the scatter of the individual data around the straight line is larger than the estimated experimental errors. Most important, the comparison suggests that the CO mixing ratios measured in the bottles, on average, are systematically lower by 12 ppb than those measured in situ, by RF. If the negative bias is subtracted, the main body of measurements agrees within 10%, although individual bottles deviate from the straight line by as much as 20%. There are several possible explanations for the observations.

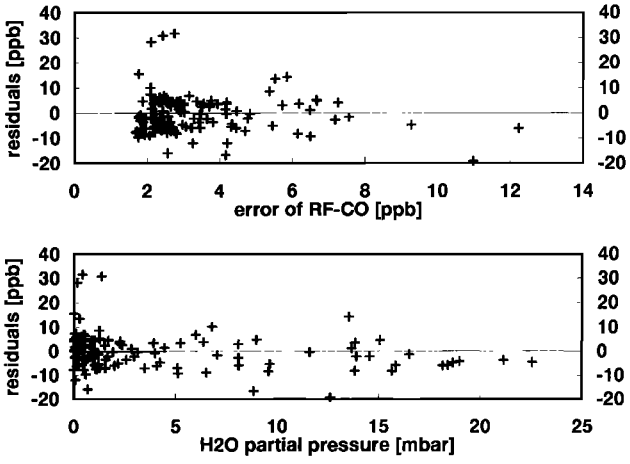

Figure 10b. Residuals plotted versus (top) the estimated error of the continuous data and versus (bottom) water vapor pressure.

Imperfect matching between the actual filling period of the bottles and the integration interval used for the continuous data can be excluded. The filling periods (typical duration 1–3 min) were exactly recorded in the flight protocol, and the signal measured by the RF instrument was averaged over that period. Only the change in the rate of filling was not taken into account for averaging the continuous data, which could result in higher residuals in case of high atmospheric variability in the CO mixing ratio during the filling period. However, the residuals show no correlation with the variability in the CO mixing ratio, as determined from the continuous measurements. Unstable background signals of the RF instrument can be excluded as well, since the residuals shown in Figure 10b show no systematic dependence on the estimated error of the continuous data, including variations in the background signal. Similarly, there is no systematic trend of the deviations with atmospheric humidity, which could point to an undetected malfunction of the water trap in the in situ measurement.

The detector used in the RGA 3 was shown to have a nonlinear response in the range below 100 ppb [*Novelli et al.*, 1994]. The respective response curve is reproduced in Figure 10. It could, in principal, explain the negative offset in the bottle analyses, although the use of a higher-order polynomial is not justified statistically, because of the large scatter in the data.

It is known that oxidation of the carbon contained in the walls of stainless steel bottles can lead to enhanced CO concentrations the bottles during the time between filling and analysis. Likewise, CO can be destroyed on the walls of stainless steel containers. *Novelli et al.* [1992] found changes in CO mixing ratios that ranged from −2.1 ppb/d to +7.4 ppb/d in stainless steel containers that had been filled with a mixture of 100 ppb CO in air. Since the time between filling and analysis of the bottles from the C130 was about 10 weeks (15 at maximum), this effect and the nonlinearity of the RGA 3 are the likely reason for both the offset of −12 ppb and the large scatter.

Vertical Profiles of CO and NO_y Over the North Atlantic

During the OCTA campaign, which started on August 24 and ended on September 1, seven flights were made over the North Atlantic. The flight routes are shown in Figure 11. Profiles of CO, NO_y, and temperature that were measured southeast of Newfoundland, in the vicinity of the Azores, and west of Portugal are shown in Figure 12.

NO_y, that is, the sum of NO_x and its oxidation products, was measured with a chemiluminescence instrument, using a gold converter [cf. *Fahey et al.*, 1985] to convert the different NO_y species to NO. The instrument is described by *Lerner et al.* [1994]. The sensitivity of the NO_y detector was 0.5 c/s ppt and the conversion efficiency of the gold converter was 90% during flights A270 and A272 and 83% during flight A268. The efficiency of the gold converter was measured in both, ambient and synthetic air, with NO_2 produced by gas phase titration from the NO standard and with HNO_3 from a thermostated and pressure-stabilized permeation tube that was calibrated by ion chromatography. Since the gold converter was mounted inside the C-130, using a 0.8-m-long perfluoralkoxy (PFA) inlet, we have also made extensive tests for potential losses of HNO_3 in the inlet. From these tests, significant inlet losses of HNO_3 were identified, which amounted to 30–50% below altitudes of 1 km. Above 3 km, losses were found to be less than 25%. The high losses in the moist ABL were confirmed by an intercomparison with the NOAA instrument aboard the NCAR King Air [*Hübler et al.*, 1994].

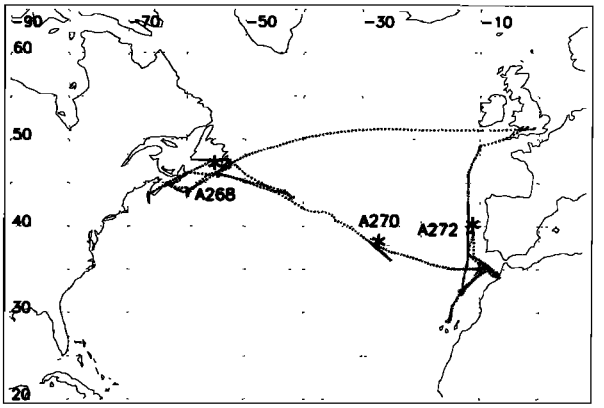

Figure 11. Flight path of the C-130 during the OCTA summer campaign in August 1993 with the locations of the vertical profiles that are discussed in the text.

Flight A268

The vertical profile sampled south of Newfoundland on August 25 shows several layers of differing CO mixing ratios. These layers are also associated with lapse rate changes or are separated by inversions in the temperature profile. The most prominent feature is a layer of high CO and NO_y mixing ratios between 1.8 and 2.5 km. The maximum CO mixing ratios are around 230 ppb and NO_y peaks at 1.8 ppb. The lapse rate in this layer (<2 K/km) is smaller than below and aloft and the relative humidity is quite low (dew point < 250 K). While the low humidity together with enhanced NO_y could point toward stratospheric origin, the high CO mixing ratios show that this air has probably originated from the ABL over the North American continent. From the dew point it is then suggested that the air has reached an altitude of approximately 8 km, most likely in a convective cell, before it was transported to the ocean and subsided to the lower free troposphere. The NO_y/CO ratio in this layer (<0.01) is about 20 times lower than the NO_x/CO emission ratio of about 0.18 for the eastern United States [*Chin et al.*, 1994]. Although a lower NO_y/CO ratio than that in fresh emissions is partially due to dilution of the emission with aged air, the very low NO_y/CO ratio observed in this layer suggests that a large fraction of the NO_y originally present was lost by heterogeneous processes, most likely through rainout.

The lowest NO_y mixing ratios are observed close to the surface in a 200-m-thick isothermal layer, which is capped by a sharp inversion. Above 4 km, the correlation between CO and NO_y disappears, and there is some evidence for stratospheric air at 5 km, where a decrease in humidity coincides with the lowest CO mixing ratio of the whole profile (70 ppb).

Flight A270

In the vicinity of the Azores, CO mixing ratios in the free troposphere were somewhat smaller than those in the boundary layer. Again, several layers are identified from temperature and dew point. The lowest CO mixing ratio of 70 ppb is found between 3.5 and 4 km. NO_y was low throughout the profile with values in the boundary layer around 250 parts per trillion by volume (pptv), some of the lowest values ever observed

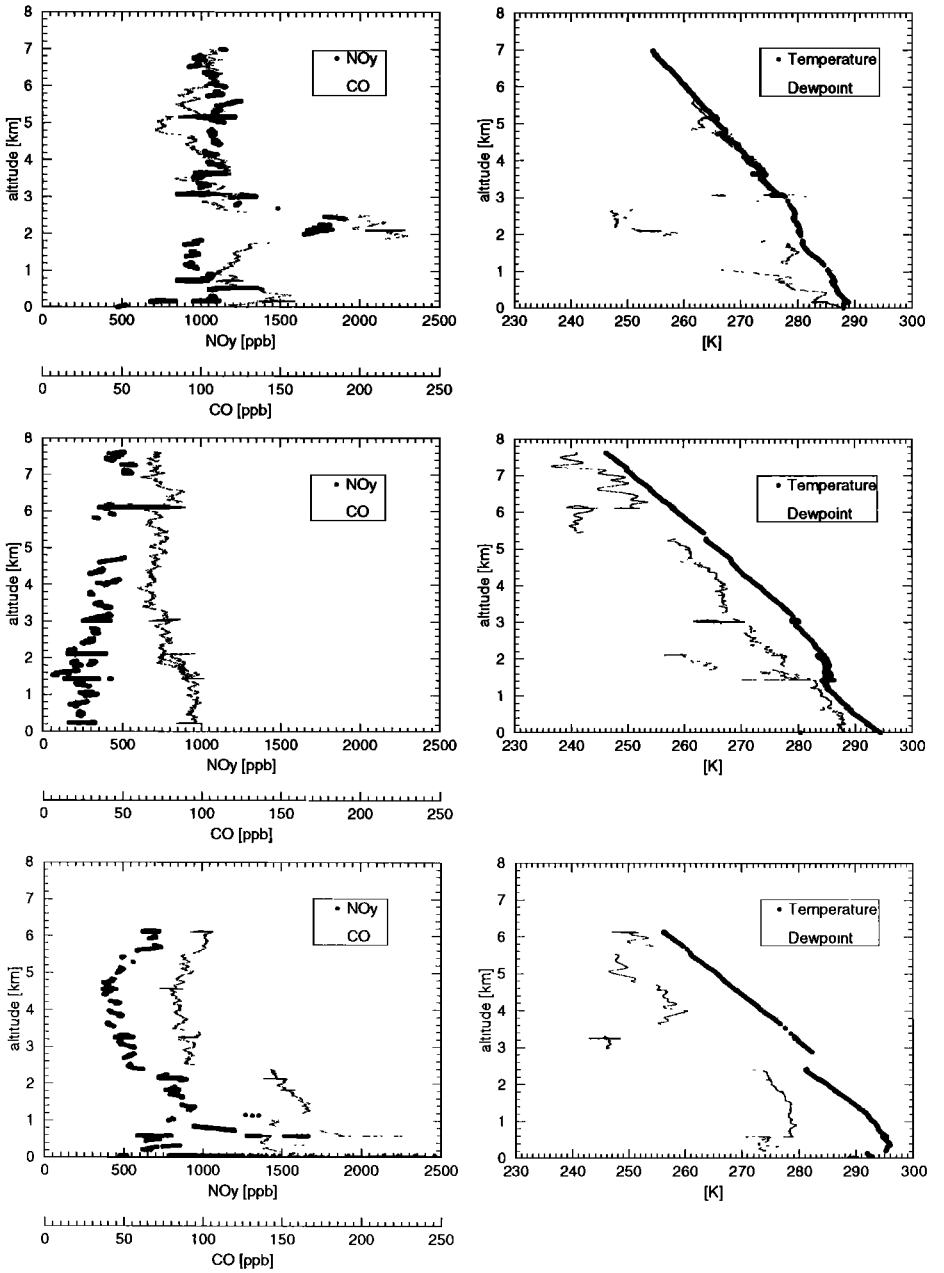

Figure 12. Vertical profiles obtained from flights (top) A268 near Newfoundland, (middle) A270 near the Azores, and (bottom) A272 near Portugal. The individual points are 16-s running means.

from the C-130, and increasing slightly with height up to almost 500 pptv near the maximum altitude. The slightly higher CO mixing ratios below 2 km and the layer of enhanced CO above 6 km might indicate an influence of long-range transport, a fact that is supported by back trajectory calculations [cf. *Wild et al.*, this issue]. Clearly, the signatures are much weaker than in the profile obtained closer to the American continent.

Flight A272

The highest mixing ratios (250 ppb of CO and 2.5 ppb of NO_y at the surface) were found in the surface layer near the coast of Portugal. There, fairly high mixing ratios of CO and NO_y persisted up to 2.5 km. Several shallow layers are seen where both CO and NO_y increase simultaneously. Trajectories suggest that these air masses are advected from the Iberian Peninsula. The large variations during times when the aircraft flew at constant altitude (for filling of bottle samples) show the large spatial inhomogeneity in a region close to areas of strong emissions, for example, the area around Lisboa. The CO mixing ratios drop sharply (within 50 m) at the strong inversion located at 2.5 km. The values in the free troposphere around 5 km are quite similar to those observed in the middle of the North Atlantic. Small-scale correlations of CO and NO_y persist through large parts of the free troposphere. The simultaneous increase of CO and NO_y at the top of the profile occurs in air masses that are advected from North America, according to back trajectory calculations. A more detailed analysis of this profile is found by *Wild et al.*, [this issue]. The two enhancements in CO, NO_y, and H_2O observed on the A270 and A272

profiles around 6 km possibly represent air which was transported vertically but which had not yet descended isentropically as it was suggested for the dry layer with high CO mixing ratios in profile A268.

Conclusions

The laboratory tests and data from flights made aboard the C-130 of the UKMO show that the RF instrument developed by A. Volz and D. Kley is well suited for airborne measurements of CO because of its high sensitivity, time resolution, and dynamic range. The time resolution of 2 s that was achieved during the flights can be improved by using a larger pump for the sample flow. Resonance Raman scattering by molecular oxygen was identified as a major source of the background signal, and interferences of water vapor were found to influence the CO measurement by absorption of the fluorescence radiation and by photofragmentation that yields OH fluorescence. For this reason, water must be removed from the sampled air to a level below 20 ppm.

The data presented from the OCTA flights clearly identify layers of high pollution in the free troposphere that are transported to the North Atlantic. The data show a considerable amount of vertical (and horizontal) structure which can only be resolved with appropriate time resolution and data coverage. A very dry layer with high NO_y and CO mixing ratios was found above the boundary layer south of the coast of Newfoundland. The low NO_y/CO ratio points toward heterogeneous losses of NO_y compounds, that is, HNO_3. It should be possible to quantify these losses in the future by determination of the chemical age of the air mass from the hydrocarbons measured simultaneously aboard the C-130. At farther distances from the source regions, signatures of long-range transport from North America, albeit much weaker, are still visible in the vertical profiles of CO.

Acknowledgments. The support that the campaign was given by the Commission of the European Community, Directorate DG XI, as part of project EV 5V-CT91-0042 (OCTA) is gratefully acknowledged. The authors like to thank the personnel of the Meteorological Research Flight Department and the aircraft crew for their assistance before and during the campaign, the technical personal of ICG for their assistance during building of the aircraft instrument, and the NOAA Aeronomy Laboratory for letting us have the prototype developed by A. Volz and D. Kley.

References

Chin, M., D. J. Jacob, J. W. Munger, D. D. Parrish, and B. G. Doddridge, Relationship of ozone and carbon monoxide over North America, *J. Geophys. Res.*, *99*, 14,565–14,573, 1994.

Dickerson, R. R., and A. C. Delany, Modification of a commercial gas filter correlation CO detector for enhanced sensitivity, *J. Atmos. Oceanic Technol.*, *5*, 424–431, 1987.

Fahey, D. W., C. S. Eubank, G. Hübler, and F. C. Fehsenfeld, Evaluation of a catalytic reduction technique for the measurement of total reactive odd-nitrogen NO_y in the atmosphere, *J. Atmos. Chem.*, *3*, 435–468, 1985.

Fink, E., Schwingungsrelaxation und Löschung elektronisch angeregter $CO(A^1\Pi)$- und $NO(A^2\Sigma^+)$-Moleküle in Stössen mit Edelgasatomen und einfachen Molekulen, Habilitationsschrift Universität Bonn, 1976.

Fishman, J., and W. Seiler, Correlative nature of ozone and carbon monoxide in the troposphere: Implications for the tropospheric ozone budget, *J. Geophys. Res.*, *88*, 3662–3670, 1983.

Heidt, L. E., Whole air collection and analysis, *Atmos. Technol.*, *9*, 3–7, 1978.

Herzberg, G., *Molecular Spectra and Molecular Structure*, vol. 1, *Spectra of Diatomic Molecules*, Van Nostrand, Reinhold, New York, 1974.

Hipskind, R. S., G. L. Gregory, G. W. Sachse, G. F. Hill, and E. F. Danielsen, Correlations between ozone and carbon monoxide in the lower stratosphere, folded tropopause, and maritime troposphere, *J. Geophys. Res.*, *92*, 2121–2130, 1987.

Hubler, G., et al., Intercomparison Activities During the NARE Summer 1993 Intensive, *EOS Trans. AGU*, *75*(44), Fall Meet. Suppl., 94, 1994.

Krupenie, P. H., The spectrum of molecular oxygen, *J. Phys. Ref. Data*, *1*(2), 423, 1972.

Lerner, A., D. Kley, A. Volz-Thomas, and D. S. McKenna, Ozon-Stickoxid-Korrelationen in der Troposphäre, *Ber. Forschungszent. Jülich, Jül-3008, ISSN 0944-2952*, Jülich, Germany, 1994.

Logan, J. A., M. J. Prather, S. C. Wofsy, and M. B. McElroy, Tropospheric chemistry: A global perspective, *J. Geophys. Res.*, *86*, 7210–7254, 1981.

Marenco, A., M. Macaigne, and S. Prieur, Meridional and vertical CO and CH_4 distributions in the background troposphere (70°N–60°S; 0–12 km altitude) from scientific aircraft measurements during the STRATOZ III experiment, *Atmos. Environ.*, *23*, 185–200, 1989.

Novelli, P. C., L. P. Steele, and P. P. Tans, Mixing ratios of carbon monoxide in the troposphere, *J. Geophys. Res.*, *97*, 20,731–20,750, 1992.

Novelli, P. C., J. E. Collins Jr., R. C. Myers, G. W. Sachse, and H. E. Scheel, Reevaluation of the NOAA/CMDL carbon monoxide reference scale and comparisons with CO reference gases at NASA-Langley and the Fraunhofer Institut, *J. Geophys. Res.*, *99*, 12,833–12,839, 1994.

Parrish, D. D., J. S. Holloway, M. Trainer, P. C. Murphy, G. L. Forbes, and F. C. Fehsenfeld, Export of North American ozone pollution to the North Atlantic Ocean, *Science*, *259*, 1436–1439, 1993.

Pickering, K. E., J. R. Scala, A. M. Thompson, W. K. Tao, and J. Simpson, Free tropospheric ozone production following entrainment of urban plumes into deep convection, *J. Geophys. Res.*, *97*, 17,985–18,000, 1992.

Sachse, G. W., G. F. Hill, L. O. Wade, and M. G. Perry, Fast-Response, high-precision carbon monoxide sensor using a tunable diode laser absorption technique, *J. Geophys. Res.*, *92*, 2071–2081, 1987.

Seiler, W., The cycle of atmospheric CO, *Tellus*, *24*, 116–135, 1974.

Seiler, W., H. Giehl, and P. Roggendorf, Detection of carbon monoxide and hydrogen by conversion of mercury oxide to mercury vapor, *Atmos. Technol.*, *12*, 40–47, 1980.

Terenin, A. N., and G. G. Neuimin, Photodissociation of molecules in the Shumann ultraviolet, *Nature*, *134*, 255, 1934.

Volz, A., and D. Kley, A resonance fluorescence instrument for the in-situ measurement of atmospheric carbon monoxide, *J. Atmos. Chem.*, *2*, 345–357, 1985.

Volz, A., D. H. Ehalt, and R. G. Derwent, Seasonal and latitudinal variation of ^{14}CO and the tropospheric concentration of OH-radicals, *J. Geophys. Res.*, *86*, 5163–5171, 1981.

Watanabe, K., and M. Zelikoff, Absorption coefficients of water vapor in the vacuum ultraviolet, *J. Opt. Soc. Am.*, *43*, 753, 1953.

Wild, O., K. S. Law, B. J. Bandy, S. A. Penkett, J. A. Pyle, and D. S. McKenna, Photochemical trajectory modelling studies of the North Atlantic region during August 1993, *J. Geophys. Res.*, this issue.

Zöller, E., Aufbau und Weiterentwicklung eines CO-Detektors basierend auf dem Prinzip der Resonanzfluoreszenz, Diplomarb. Fachhochsch. Aachen, Germany, 1995.

K. Dewey, J. Kent, and D. S. McKenna, Atmospheric Chemistry Group, Meteorological Research Flight, UKMO, Defense Research Agency, Farnborough, Hampshire, GU146 TD, UK.

C. Gerbig, D. Kley, and A. Volz-Thomas, Institut fur Chemie und Dynamik de Geosphäre, Institut 2, Chemie der Belasteten Atmosphere, Forschungszentrum Julich GmbH ICG-2, D-52425 Julich, Germany.

(Received May 25, 1995; revised October 2, 1995;
accepted October 2, 1995.)